Final Technical Report, USGS National Earthquake Hazard Reduction Program

Systematic tests of asymmetric propagation directions of earthquakes on Southern CA faults based on large seismic catalog datasets.

Yehuda Ben-Zion
Department of Earth Sciences
University of Southern California, Los Angeles, CA, 90089-0740
phone: (213) 740-6734; fax (213) 740-8801
e-mail: benzion@usc.edu

Danijel Schorlemmer
Department of Earth Sciences
University of Southern California, Los Angeles, CA, 90089-0740
phone: 213-740-4141; fax (213) 740-8801
e-mail: ds@usc.edu

External grant award number: G09AP00019
Program element: III

Start date: January 1, 2009
End date: December 31, 2009

Abstract
The directivity of earthquake ruptures can have significant effects on the spatial distribution of the generated ground shaking and associated seismic hazard. Theoretical studies suggest that rupture on faults that juxtapose different elastic solids evolve for a wide range of conditions toward asymmetric rupture, with a preferred propagation direction that is controlled by the velocity contrast across the fault. The studies done under this project attempted to develop and apply techniques for analyzing correlations between along-strike asymmetry of seismicity, which may imply preferred propagation direction of earthquake ruptures, and information on the velocity structures of the faults. The studies involved two separate research directions. In the first direction, Schorlemmer and Ben-Zion investigated symmetry properties of dynamic triggering patterns of seismicity along the Northern San Andrews fault, with a focus on robustness of previously obtained results on the employed catalog, location errors, and calculation technique. The analysis indicates that the previously used technique is very sensitive to errors and uncertainties, since the number of events associated with dynamic triggering of low-magnitude earthquakes is very small. We are currently attempting to change the counting and normalization methods to obtain more stable and robust results. In the second research direction, Zaliapin and Ben-Zion examined the relations between spatial symmetry properties of seismicity along twenty five faults in CA and local velocity structure images. The analysis employs stacked signals based on aftershocks in close space-time proximity to the parent (triggering) events. We first distinguish between clustered and homogeneous parts of each catalog using a recently introduced earthquake cluster analysis, calculate an asymmetry index for the clustered portion of each examined catalog, and stack the results to obtain a cumulative asymmetry index. The results indicate strong asymmetric patterns in early-time spatially-close aftershocks along large faults with prominent bimaterial interfaces (*e.g.*, sections of the San Andreas fault), with enhanced activity in the directions predicted for the local velocity contrasts, and absence of significant asymmetry along most other faults. Assuming the observed asymmetric properties of seismicity reflect asymmetric properties of earthquake ruptures, the discussed methodology and results can be used to develop refined estimates of seismic shaking hazard associated with individual fault zones.

Asymmetric along-strike earthquake directivities on the northern San Andreas fault

(Schorlemmer and Ben-Zion, work in progress)

We investigated the results, as reported in the proposal, for stability and dependence on the particular catalog. In a first step, we repeated the calculation with a catalog of relocated events for the same area. We were not able to reproduce the results, in contrary, the signal looked quite different. We investigated the catalog and found that this catalog contained events not present in the original catalog and concluded that this catalog may well be flawed significantly. However, we were aware that the different signal could also be caused by instabilities due to our procedure rather than the dataset used. Therefore, we investigated in detail the signal based on the original catalog. We computed the contributions of each triggering earthquake to the resulting signal and investigated for each point in the asymmetry plots which and how many earthquakes contributed significantly. We found that in many cases the signal is dominated by very few events that contribute very strongly to the resulting asymmetry values. This sometimes supports the many little contributions of the other earthquakes but we also find cases in which the little contributions show a different trend but are overruled by contributions from few earthquakes.

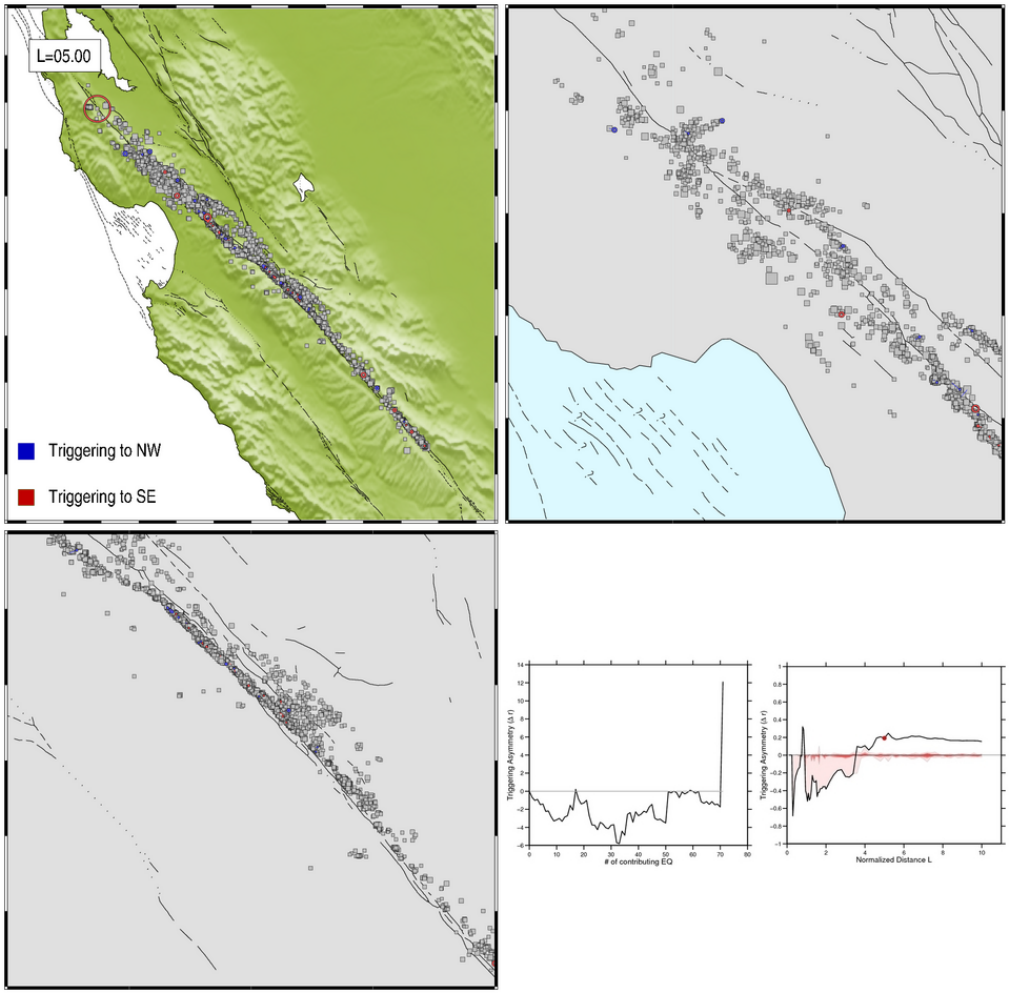

Fig 1: Contributions of triggering events.

Figure 1 shows such an effect. The two frames in the bottom right corner show the triggering asymmetry. In the right frame, one can see the triggering asymmetry as a function of the normalized rupture distance as derived from the event magnitudes. A positive and negative signal indicate more triggering to the south-east and north-west, respectively. The red dot indicates the normalized distance L for which the plot to the left was computed. It shows in a cumulative sense how much the around 70 earthquakes and their following triggered events contribute to the signal. It can be clearly seen that one signal completely determines the signal and that the signal would by negative without this event. The map in top left corner highlights all these 70 events in colors indicating their asymmetry contribution.

We found that the method used to compute the asymmetry was causing these computational artifacts. The asymmetry was computed as the rate of triggered events over the estimated background rate of events in the particular area of the triggering event. In the case of small time periods and very low background rates, the asymmetry can reach very large values, indicating rather a combination of short periods of investigation than a strong triggering signal. Because the asymmetry signals of all triggering earthquakes were stacked uniformly, one large value happened to determine the entire signal. We further found a problem with events not having triggered events. Although we were normalizing all triggering based on the observed background rate at each location, events that had no triggered earthquakes did not contribute at all. Hence, the background rate was not appropriately taken into account for this class of events.

To account for these problems, we changed the asymmetry computation. We decided to stack the triggered events first and to determine the asymmetry from these stacks. This approach removes the strong dependency of asymmetry values from single events with large values. As in the previous method, we first define a normalized distance and period after an potentially triggering events. We search the catalog for all qualifying events and stack the number of triggered events in both directions. Simultaneously, we compute the background rate of both volumes (one volume in each directions) as the number of observed earthquakes in these volumes. The ratio of triggered events to the south-east is then compared to the sum of triggered events in both direction. A value over 0.5 indicates preferential triggering to the south-east.

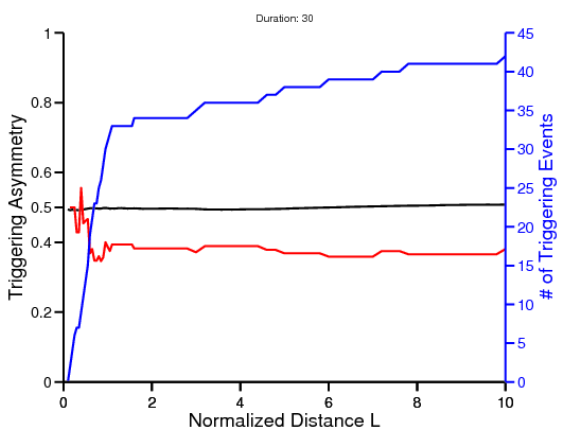

Fig 2: Triggering asymmetry using the new method (30s)

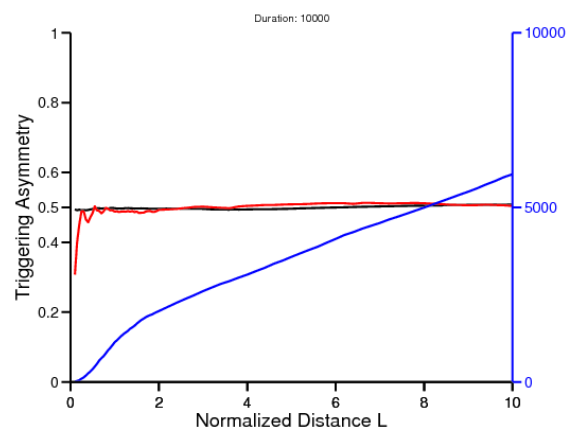

Fig 3: Triggering asymmetry using the new method (10000s)

Figures 2 and 3 show the signal obtained with the new method. The red lines indicate the triggering asymmetry and the black lines the background asymmetry of seismicity. The blue lines indicate the cumulative number events considered with increasing normalized distance L.

For short periods (e.g. 30s) the signal shows a clear triggering pattern to the north-west, while for longer periods (e.g. 10000s) we observe slight triggering to the southeast.

We also looked into the stability of this approach and added location uncertainties to the catalog. Because the magnitudes of earthquakes used in this study are very small, which then translates into small rupture lengths, adding uncertainties could easily dominate the signal. The signal vanishes when applying moderate uncertainties to the event locations. Further investigations are underway.

Asymmetric distribution of early aftershocks on large faults in California

(Zaliapin and Ben-Zion, 2010)

Symmetry properties of seismicity

In this study, we first detect significant earthquake clusters defined as the groups of earthquakes that happen unusually close to a parent earthquake in a given space-time domain. The asymmetry analysis is then done only for these pre-defined parent-children sequences. The principal novelty of our approach is in identifying significant clustered sequences. The main tool in solving this problem is an appropriate definition of the distance between earthquakes. We use and further develop here the distance suggested by *Baiesi and Paczuski* (2004) for studying aftershock clustering.

Consider an earthquake catalog, where each event i is characterized by its occurrence time t_i, hypocenter (ϕ_i, λ_i, d_i), and magnitude m_i. The triggering approach motivates us to consider distance between earthquakes i and j that is asymmetric in time:

$$\eta_{ij} = \begin{cases} t_{ij}(r_{ij})^d 10^{-bm_i}, & t_{ij} > 0; \\ \infty, & t_{ij} \le 0. \end{cases} \tag{1}$$

Here, $t_{ij} = t_j - t_i$ is the intercurrence time, which takes positive values if earthquake i happened before earthquake j and negative values otherwise, $r_{ij} \ge 0$ is the spatial distance between the earthquake hypocenters, and d is the (possibly fractal) dimension of the space containing the earthquake hypocenters.

Zaliapin et al. (2008) expanded a study of the scalar distance η to a more focused analysis of the joint distribution of the distance's spatial and temporal components. Specifically, they considered the space and time distances between the nearest neighbors normalized by the magnitude of the earlier event:

$$T_{ij} = t_{ij} 10^{-qbm_i};\ R_{ij} = (r_{ij})^d 10^{-pbm_i};\ q + p = 1. \tag{2}$$

It is readily seen that $\log \eta_{ij} = \log T_{ij} + \log R_{ij}$. These authors demonstrated a prominent bimodal joint distribution of (log T, log R), with one mode corresponds to a homogeneous Poisson process, while the other – to the presence of a large subpopulation of events located significantly closer in time and space to their parents than expected in a Poisson process with no clustering.

For each earthquake j in the catalog, we identify its nearest neighbor i and the nearest-neighbor distance η_{ij}. As a result, each earthquake has a single parent (the nearest neighbor), and any given earthquake can be the parent for multiple children events. Next, we analyze the 2D joint distribution of the time and space components of the nearest-neighbor distance. To make the results directly comparable for parent events of different magnitudes, we normalize the spatial component of the distance by the rupture length L_M of the parent event with magnitude M (*Ben-Zion*, 2008):

$$R_{ij} = \frac{r_{ij} 10^{-pbm_i}}{0.0152}, \tag{3}$$

with p = 0.42, which differs from the general definition (2) only by the constant 0.0152. Formally, we use the following formal threshold definition of clustered event:

$$R_{ij} < R_0, T_{ij} < T_0, \text{ and } m_j < m_i \tag{4}$$

with appropriately chosen values for the thresholds R_0 and T_0. Only clustered events are considered for future analysis.

We have analyzed spatio-temporal properties of seismicity along twenty five fault zones (Figure 4) defined by *Powers and Jordan* (2009). For each child-earthquake j within the clustered sequence, we define S_{ij} as the *signed normalized distance* from this earthquake to its parent i. The degree of asymmetry of a given earthquake cluster is measured by the following asymmetry index:

$$I_A = \sqrt{n}\,\frac{mean(S)}{st.dev(S)} \tag{5}$$

where $S=\{S_{ij}\}$, $j = 1,\ldots,n$ is the sample that consists of all spatial signed distance components in the cluster. In each zone, we identified significant clusters according to the criterion (4) and computed the asymmetry index (5) for each clustered sequence.

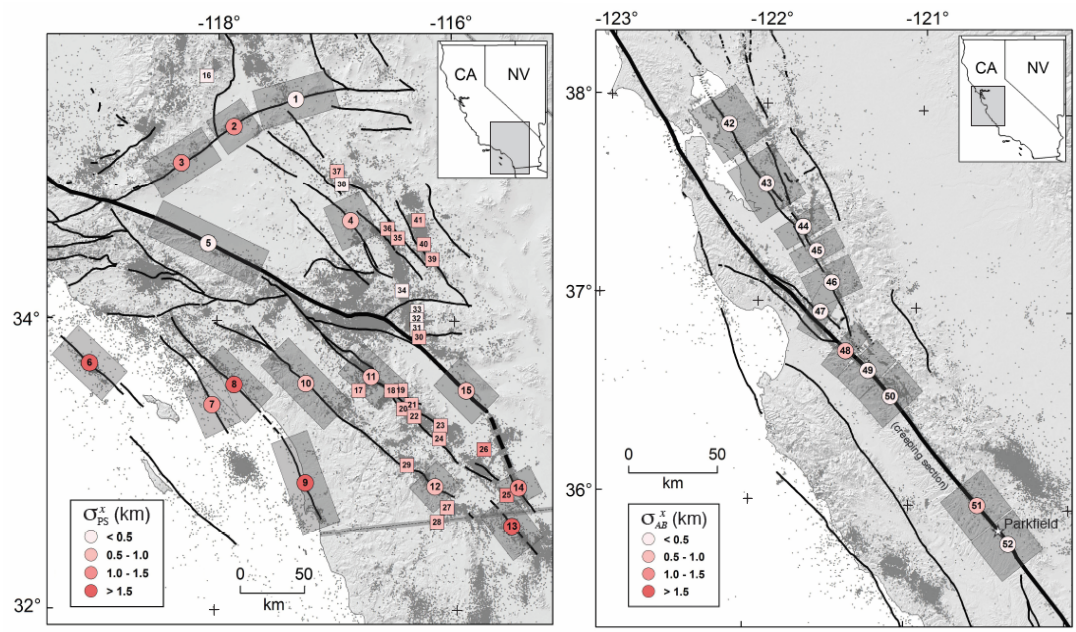

Figure 4. Location map of seismically active fault zones. The zone indexes in circles indicate regions analyzed in this study, while the zone indexes in squares indicate aftershock-dominated zones that are not analyzed here [After *Powers and Jordan* (2009)].

To characterize the overall asymmetry of seismicity in a given zone, we use the weighted average of the values A_k from all individual clusters. It should be noted that most of the clusters consist of only a couple of events, and using them in evaluating seismic distribution asymmetry is inefficient. We therefore use only clusters with more than 5 events, meaning that the weight of a cluster with less than 5 events is set to zero. The weights of the other clusters are made proportional to the number of events within a cluster. Finally, the zonal asymmetry index A is computed as

$$A = \frac{\sum A_k N_k}{\sum N_k} \quad , \tag{6}$$

where A_k is the asymmetry index for cluster k comprised of N_k events and the summation is taken over all clusters with more than 5 events.

Fault velocity contrasts

Summarizing information on the velocity contrasts across the examined faults is not straightforward, because of non-uniformity of the available data and their resolution. Nevertheless, it is possible to make a coarse classification into the following two categories. (1) Cases where the existing evidence indicate average velocity contrast of 5% or more that is persistent over distances of several tens of km or more are labeled "strong contrast". (2) Cases where imaging studies indicate no contrast or possible mild contrasts that are likely to exist only in sub-sections of the zone and mixed with other sections of no contrast are labeled "no-to-mild contrast". We note that this latter category includes zones where there is evidence for two or more faults with reversed velocity contrasts, or reversal in the sense of contrast along strike and/or depth, which are expected to produce opposite effects on statistical results. This category also includes cases with limited imaging information, since it is more likely for a randomly chosen fault to have no-to-mild contrast.

In classifying the zones into one of the forgoing categories we use the highest available resolution results on bimaterial fault interfaces in the seismogenic zone (*e.g.*, depth range of 3-15 km). The most informative signals are those associated with fault zone head waves that propagate along, and hence owe their existence to, velocity contrast interfaces (*e.g., Ben-Zion,* 1989, 1990; *Lewis et al.,* 2007; *Zhao et al.*, 2010). In places where head waves studies have not been done we use, in this order, (i) results of reflection/refraction studies that focus on clarifying near-fault structures (*e.g.*, *Fuis et al.,* 2003) and (ii) local and regional tomographic studies (*e.g.*, *Eberhart-Phillips and Michael,* 1998; *Tape et al.,* 2009). The classification of the zones to the different categories can be as follows.

Zones 1 and 2: No contrast based on the regional tomography of *Tape et al.* (2009). The web site <http://www.data.scec.org/research/carltape/socalm16.html> gives various cross sections of the 3-D imaged of *Tape et al.* (2009).

Zone 3: Possible mild contrast with faster NW side (*Tape et al.*, 2009).

Zones 4, 7, 8, 13, 14: No contrast (*Tape et al.*, 2009).

Zone 5: Clear contrast with faster NE side based on seismic reflection imaging (*Fuis et al.*, 2003).

Zone 9: Possible contrast with faster NE side (*Tape et al.*, 2009).

Zone10: No contrast to possible mid contrast with faster SW side (*Tape et al.*, 2009).

Zone 11: Mild contrast with faster NE side based on local tomographic study (*Scott et al.*, 1994).

Zone 12: Mild contrast with faster NE side (*Tape et al.*, 2009).

Zone 15: Clear contrast with faster SW side (*Tape et al.*, 2009).

Zone 42: Clear contrast with faster NE side based on head waves study (*Ohlendorf et al.*, 2007) and regional tomography (*Thurber et al.*, 2007).

Zone 43: Mild contrast with faster NE side (*Ohlendorf et al.*, 2007; *Thurber et al.*, 2007).

Zone 44: Mild contrast with faster SW side based on tomography studies (*Michael and Eberhart-Phillips*, 1991; *Thurber et al.*, 2007).

Zone 45: Mild average contrast with faster NE side based on local tomography (*Michael and Eberhart-Phillips,* 1991) and head wave study (*Zhao and Peng*, 2008).

Zone 46: No contrast based on tomography studies (*Eberhart-Phillips and Michael*, 1998; *Thurber et al*., 2007).

Zone 47: No contrast to possible mid contrast with faster SW side (*Eberhart-Phillips and Michael,* 1998).

Zone 48: Clear contrast with faster SW side based on head wave studies (*McGuire and Ben-Zion*, 2005; *Lewis et al.*, 2007) and local tomography (*Thurber et al.*, 1997).

Zones 49, 50: No to mild average contrast owing to seismicity in these zones on interfaces with opposite velocity contrasts (*McGuire and Ben-Zion*, 2005).

Zone 51: Clear contrast with faster SW side based on head wave studies (*Ben-Zion et al.*, 1992; *Zhao et al.*, 2010) and local tomography (*Eberhart-Phillips and Michael, 1993; Thurber et al.*, 2006).

Zone 52: Minor average contrast based on the head- wave study of *Zhao et al.* (2010) and local tomography (*Eberhart-Phillips and Michael*, 1993; *Thurber et al.*, 2006).

Results

The distribution of asymmetry indices in all 25 zones is summarized in Figure 5. For each zone we show the index mean (solid circle) and error bars that span the range between the 5% and 95% empirical percentiles of the asymmetry index sample. Hence, the 90% (or 1771 out of 1968) of asymmetry indices lie within the error bars. Fig. 5 orders the zones according to our assessment of the degree of velocity contrast: zones 5, 15, 42, 48, 51 have clear velocity contrasts and are followed by the other zones which have no-to-mild contrast.

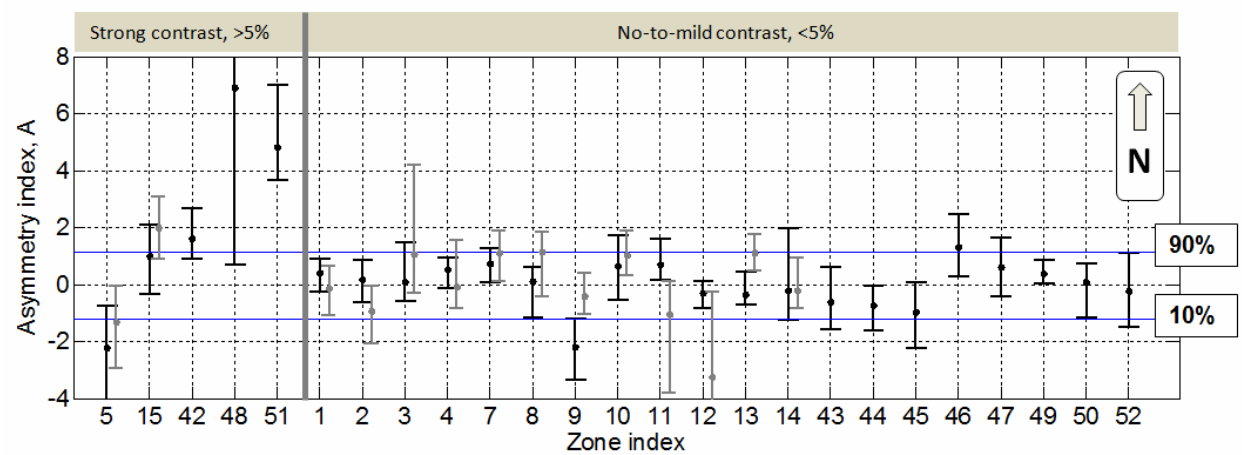

Figure 5. Asymmetry results for 25 fault zones considered in the study. Dots depict the mean values of zonal asymmetry index *A* (Eq. 6). The error bars show the range between 5% and 95% empirical percentiles of the asymmetry index distribution for 1968 estimations with different parameter values (see text for details). Horizontal lines mark 10% and 90% empirical quantiles of the asymmetry index distribution within 20 no-to-mild contrast zones, and provide a guide for assessing significance of the asymmetry. Black and gray symbols correspond, respectively, to the catalogs of *Shearer et al.* (2005) and *Hauksson and Shearer* (2005) in southern California. For northern California faults, the relocated catalog of *Ellsworth et al.* (2000) is used. Positive values correspond to northward asymmetry (NE or NW), while negative values correspond to southward asymmetry (SE or SW).

To roughly assess the significance of the asymmetry index, we show in Fig. 5 by horizontal lines the empirical 10% and 90% percentiles of the *A*-values computed only within no-to-mild contrast zones. Zones where the average asymmetry index is lying outside of the

range depicted by the horizontal lines can be considered significantly asymmetric. We emphasize that we are not trying to define a formal significance criterion for this problem, which is a hard task due to various complications of analysis and data sets (mainly, serious dependence among the *A*-values in the same zone), but rather suggest the empirical bounds as a convenient visual tool. One can readily see that *all* zones with strong velocity contrast have asymmetry indices outside of the empirical bounds; while most of the zones with no-to-mild contrast have asymmetry index within the bounds. Below we compare in more detail the obtained results with the available images of the velocity contrasts and other relevant information.

Strong contrast zones

Notably, all five zones with a well-established strong velocity contrast (zones 5, 15, 42, 48, and 51) exhibit strong asymmetry in the direction consistent with the theoretical predictions based on the reported velocity contrasts. For instance, in zone 48 (creeping section of the SAF south of Hollister) and zone 51 (creeping SAF section just north of Parkfield), the strong NW asymmetry is consistent with seismic imaging of the velocity contrast based on head waves and local tomography (*e.g.*, *McGuire and Ben-Zion*, 2005; *Thurber et al.*, 2006; *Ben-Zion et al.*, 1992). The results in zone 48 are also consistent with similar findings of *Rubin and Gillard* (2000) and seismic imaging results on asymmetric rock damage (*Lewis et al*., 2007). In zone 5 (the Mojave section of the SAF), the SE asymmetry is consistent with evidence (*e.g.*, *Fuis et al.,* 2001) for a "reversed" velocity contrast compared to the central section of the SAF (with the NE block having faster velocity) and field observations of asymmetric rock damage in that section (*Dor et al.*, 2006a,b).

No-to-mild contrast zones

Most of the zones in this category show indeed no-to-mild values of the asymmetry index *A*. In particular, it is interesting to note the lack of asymmetry in zone 52 (creeping SAF section just south of Parkfield) that stands in marked contrast with the strong asymmetry in the neighboring zone 51 north of Parkfield. The lack of asymmetry in zone 52 is consistent with the near zero average velocity contrast in that section based on high resolution head waves and local tomography imaging studies (*Zhao et al*., 2010; *Thurber et al.*, 2006; *Eberhart-Phillips and Michael*, 1993). We discuss below, one by one, zones that show significant asymmetry for at least one catalog. Notably, only two of the 20 no-to-mild contrast zones show behavior that is inconsistent with the predictions based on the velocity contrasts.

Zone 3 (western section of the Garlock fault) shows a somewhat NE asymmetry when using the *Hauksson and Shearer* (2005) catalog. This is not consistent with a mild velocity contrast with faster NW side, based on the regional tomography results of *Tape et al.* (2009) at depths around 5 km which corresponds to the average seismic depth in this zone. A number of mechanisms may produce a competing effect to the velocity contrast that may be responsible for the discrepancy. Examples include fault curvature or dip, permeability contrast around the rupture zone with reserved sense from that of the elastic contrast (*Rudnicki and Rice*, 2006; *Dunham and Rice*, 2008), persistent stress concentration at the NE portion of zone 3, perhaps due to proximity to faults of the Eastern CA shear zone, or another source that produces enhanced hypocenter production to the NE. It is also possible that there exists a local velocity contrast across the fault with faster SE side that is not resolved by the regional tomography imaging.

Zone 9 (south Newport Inglewood) shows significant SE asymmetry for the *Shearer et al.* (2005) catalog, which is consistent with a velocity contrast with faster NE side at the depth of 10 km reported by *Tape et al.* (2009). The average seismicity depth in this zone is 9.82 km.

Zone 11 (San Jacinto) shows a tendency to SE asymmetry for the *Hauksson and Shearer* (2005) catalog that is consistent with seismic imaging of the velocity contrast in this region (*Scott et al.,* 1994) and asymmetric rock damage based on trapped waves (*Lewis et al.*, 2005) and geologic information (*Dor et al.,* 2006a; *Wechsler et al.,* 2009).
Zone 12 (Ellsinore) shows SE asymmetry for the *Hauksson and Shearer* (2005) catalog that is consistent with the velocity profile of *Tape et al.* (2009) at the depth of 10 km. The average seismicity depth in this zone is 9.91 km.
Zone 46 (southern Calaveras) exhibits a possible tendency to NW asymmetry. This may, perhaps, reflect persistent high stress concentration and hypocenters production at the SE end of the zone near the intersection with the SAF, or one of the other mechanisms noted for zone 3.

The research discussed in this section is described in more detail in a paper submitted to *Geophys. J. Int*. (Zaliapin and Ben-Zion, 2010). The paper can be downloaded from http://earth.usc.edu/~ybz/pubs_recent/ZBZ_GJI10/

References

Baiesi, M and M. Paczuski, 2004, Scale-free networks of earthquakes and aftershocks. *Phys. Rev. E*, 69, 066106.

Ben-Zion, Y., 1989, The response of two joined quarter spaces to SH line sources located at the material discontinuity interface, *Geophys. J. Int*., 98, 213-222.

Ben-Zion, Y., 1990, The response of two half spaces to point dislocations at the material interface, *Geophys. J. Int.,* 101**,** 507-528.

Ben-Zion, Y., 2008. Collective Behavior of Earthquakes and Faults: Continuum-Discrete Transitions, Evolutionary Changes and Corresponding Dynamic Regimes, *Rev. Geophysics*, 46, RG4006, doi:10.1029/2008RG000260.

Ben-Zion, Y., S. Katz and P. Leary, 1992, Joint inversion of fault zone head waves and direct P arrivals for crustal structure near major faults, *J. Geophys. Res*, 97, 1943-1951.

Dor O., T. K. Rockwell and Y. Ben-Zion, 2006a, Geologic observations of damage asymmetry in the structure of the San Jacinto, San Andreas and Punchbowl faults in southern California: A possible indicator for preferred rupture propagation direction, *Pure Appl. Geophys.*, 163, 301-349.

Dor O., Y. Ben-Zion, T. K. Rockwell and J. Brune, 2006b, Pulverized Rocks in the Mojave section of the San Andreas Fault Zone, *Earth Planet. Sci. Lett*., 245, 642-654.

Eberhart-Phillips, D. & Michael, A.J., 1993. Three-dimensional velocity structure, seismicity, and fault structure in the Parkfield region, central California, *J. Geophys. Res.*, **98**, 15,737–15,758.

Eberhart-Phillips, D. and A. J. Michael, 1998, Seismotectonics of the Loma Prieta, California, region determined from three-dimensional V_p, V_p/V_s, and seismicity, *J. Geophys. Res.*, 103, 21099–21120.

Ellsworth, W. L., et al. (2000), Seismicity of the San Andreas Fault system in central California: Application of the double-difference location algorithm on a regional scale, *Eos Trans. AGU*, *81*(48), Fall Meet. Suppl., Abstract S21D-01.

Fuis, G.S., Ryberg, T., Godfrey, N., Okaya, D.A., and Murphy, J.M., 2001, Crustal structure and tectonics from the Los Angeles basin to the Mojave Desert, southern CA. *Geology*, 29, 15-18.

Fuis, G.S., Clayton, R.W., Davis, P.M., Ryberg, T., Lutter, W.J., Okaya, D.A., Hauksson, E., Prodehl., C., Murphy, J.M., Benthien, M.L., Baher, S.A., Kohler, M.D., Thygesen, K., Simila, G., and Keller, G.R., 2003, Fault systems of the 1971 San Fernando and 1994 Northridge earthquakes, southern California: Relocated aftershocks and seismic images from LARSE II. *Geology, 31,* 171-174.

Hauksson, E., and P. M. Shearer, 2005, Southern California hypocenter relocation with waveform cross-correlation, Part 1: Results using the double-difference method, *Bull. Seismol. Soc. Am.*, 95(3), 896–903.

Lewis, M.A, Z. Peng, Y. Ben-Zion and F. Vernon, 2005, Shallow seismic trapping structure in the San Jacinto fault zone, *Geophys. J. Int*., 162, 867–881.

Lewis, M.A, Y. Ben-Zion and J. McGuire, 2007, Imaging the deep structure of the San Andreas Fault south of Hollister with joint analysis of fault-zone head and direct P arrivals, *Geophys. J. Int.*, 169, 1028–1042.

McGuire, J. and Y. Ben-Zion, 2005, High-resolution imaging of the Bear Valley section of the San Andreas Fault at seismogenic depths with fault-zone head waves and relocated seismicity, *Geophys. J. Int.*, 163, 152-164, doi: 10.1111/j.1365-246X.2005.02703.x.

Michael, A. J., and D. Eberhart-Phillips, 1991, Relations among fault behavior, subsurface geology, and three-dimensional velocity models, *Science*, 253, 651-654.

Ohlendorf, S., Z. Peng, and Y. Ben-Zion, 2007, Velocity contrast along the Hayward fault from analysis of fault zone head waves, *Eos Trans. AGU*, 88(52), Fall Meet. Suppl., Abstract S21A-0237.

Powers, P. M. and T. H. Jordan, 2009, Distribution of Seismicity Across Strike-Slip Faults in California, *J. Geophys. Res*, in press.

Rubin, A. and D. Gillard, 2000, Aftershock asymmetry/rupture directivity along central San Andreas fault microearthquakes, *J. Geophys. Res*., 105, 19,095-19,109.

Schorlemmer, D. and Y. and Ben-Zion, 2008, Directivity effects of fault velocity contrast on triggered seismicity, *Seism. Res. Lett*., 79 (2), 295.

Scott, J.S., Masters, T.G. and Vernon, F.L. 1994, 3-D velocity structure of the San Jacinto fault zone near Anza, California – I. P waves. *Geophys. J. Int*., 119, 611-626.

Shearer, P. M., E. Hauksson, and G. Lin (2005), Southern California hypocenter relocation with waveform cross-correlation, Part 2: Results using source-specific station terms and cluster analysis, *Bull. Seismol. Soc. Am*., 95(3), 904–915.

Tape, C., Q. Liu, A. Maggi, and J. Tromp, 2009, Adjoint tomography of the southern California crust, *Science*, v. 325, p. 988-992.

Thurber, C. H., T. M. Brocher, H. Zhang, and V. E. Langenheim, 2007, Three-dimensional P wave velocity model for the San Francisco Bay region, California, *J. Geophys. Res.*, 112, B07313, doi:10.1029/ 2006JB004682.

Thurber, C., S. Roecker, W. Ellsworth, Y. Chen, W. Lutter, and R. Sessions, 1997, Two-dimensional seismic image of the San Andreas Fault in the Northern Gabilan Range, central California: Evidence for fluids in the fault zone, *Geophys. Res. Lett.*, **24**, 1591-1594.

Thurber, C.H., Zhang, H., Waldhauser, F., Hardebeck, J., Michael, A. & Eberhart-Phillips, D., 2006, Three-dimensional compressional wavespeed model, earthquake relocations, and focal mechanisms for the Parkfield, California, region, *Bull. Seismol. Soc. Am.*, **96**(4B), S38-S49, doi: 10.1785/0120050825.

Wechsler, N., T. K. Rockwell and Y. Ben-Zion, 2009, Analysis of rock damage asymmetry from geomorphic signals along the trifurcation area of the San-Jacinto Fault, *Geomorphology*, doi:10.1016/j.geomorph.2009.06.007.

Zaliapin, I., A. Gabrielov, H. Wong, and V. Keilis-Borok, 2008, Clustering analysis of seismicity and aftershock identification, *Phys. Rev. Lett*., 101.

Zhao, P. and Peng, Z., 2008, Velocity contrast along the Calaveras fault from analysis of fault zone head waves generated by repeating earthquakes, *Geophys. Res. Lett.*, 35, L01303, doi:10.1029/2007GL031810.

Zhao, P., Z. Peng, Z. Shi, M. Lewis and Y. Ben-Zion, 2010, Variations of the Velocity Contrast and Rupture Properties of M6 Earthquakes along the Parkfield Section of the San Andreas Fault, Geophys. J. Int., doi: 10.1111/j.1365-246X.2009.04436.x, 765–780.

Publications Supported by this Proposal

Zaliapin, I. and Y. Ben-Zion, Asymmetric distribution of early aftershocks on large faults in California, *Geophys. J. Int*., in review, 2010.